The impact of resolution on meteorological, chemical and aerosol properties in regional simulations with WRF-Chem

P. Crippa[1], R. C. Sullivan[2], A. Thota[3], S. C. Pryor[2,3]

[1]COMET, School of Civil Engineering and Geosciences, Cassie Building, Newcastle University, Newcastle upon Tyne, NE1 7RU, UK

[2]Department of Earth and Atmospheric Sciences, Bradfield Hall, 306 Tower Road, Cornell University, Ithaca, NY 14853, USA

[3]Pervasive Technology Institute, Indiana University, Bloomington, IN 47405, USA

Correspondence to: P. Crippa (paola.crippa@ncl.ac.uk), School of Civil Engineering and Geosciences, Cassie Building, Room G15, Telephone: +44 (0)191 208 5041, Newcastle University, Newcastle upon Tyne, NE1 7RU, UK

Abstract

Limited area (regional) models applied at high resolution over specific regions of interest are generally expected to more accurately capture the spatio-temporal variability of key meteorological and climate parameters. However, improved performance is not inevitable, and there remains a need to optimize use of numerical resources, and to quantify the impact on simulation fidelity that derives from increased resolution. The application of regional models for climate forcing assessment is currently limited by the lack of studies quantifying the sensitivity to horizontal spatial resolution and the physical-dynamical-chemical schemes driving the simulations. Here we investigate model skill in simulating meteorological, chemical and aerosol properties as a function of spatial resolution, by applying the Weather Research and Forecasting model with coupled Chemistry (WRF-Chem) over eastern North America at different resolutions. Using Brier Skill Scores and other statistical metrics it is shown that enhanced resolution (from 60 to 12 km) improves model performance for all of the meteorological parameters and gas phase concentrations considered, in addition to both mean and extreme Aerosol Optical Depth (AOD) in three wavelengths in the visible relative to satellite observations, principally via increase of potential skill. Some of the enhanced model performance for AOD appears to be attributable to improved simulation of meteorological conditions (notably precipitation and near-surface specific humidity) and the concentration of key aerosol precursor gases (e.g. SO_2 and NH_3).

Keywords: added value, high-resolution WRF-Chem simulations, precipitation, aerosol optical properties, extreme AOD

1 Motivation and Objectives

Aerosols alter Earth's radiation balance primarily by scattering or absorbing incoming solar radiation (direct effect, dominated by accumulation mode (diameters ~ wavelength (λ), where total extinction is often quantified using AOD), or regulating cloud formation/properties by acting as cloud condensation nuclei (CCN) (indirect effect, dominated by diameters $\geq$ 100 nm, magnitude = f(composition)). Most aerosols (excluding black carbon) have a larger scattering cross-section than absorption cross-section, and act as CCN thus enhancing cloud albedo and lifetimes. Hence increased aerosol concentrations are generally (but not uniformly) associated with surface cooling (offsetting a fraction of greenhouse gas warming) (Boucher, 2013;Myhre et al., 2013b) to a degree that is principally dictated by the aerosol concentration, size and composition, in addition to the underlying surface and height of the aerosol layer (McComiskey et al., 2008). Despite major advances in measurement and modeling, both the current global mean aerosol direct effect (possible range: -0.77 to +0.23 W m^{-2}) and the indirect effect (possible range: -1.33 to -0.06 W m^{-2}) remain uncertain (Stocker, 2013), as does their future role in climate forcing (Rockel et al., 2008) and regional manifestations (Myhre et al., 2013a). Specific to our current study region (eastern N. America), one analysis using the NASA GISS global model found that the "regional radiative forcing from US anthropogenic aerosols elicits a strong regional climate response, cooling the central and eastern US by 0.5–1.0 °C on average during 1970–1990, with the strongest effects on maximum daytime temperatures in summer and autumn. Aerosol cooling reflects comparable contributions from direct and indirect radiative effects" (Leibensperger et al., 2012). A recent comparison of multiple global models conducted under the AEROCOM-project indicated this is also a region that exhibits very large model-to-model variability in simulated AOD (<AOD> ~ 0.5, σ(AOD) ~ 1) (Myhre et al., 2013a).

Major reasons why aerosol radiative forcing on both the global and regional scales remains uncertain include short atmospheric residence times and high spatio-temporal variability of aerosol populations, and the complexity of the processes that dictate aerosol concentrations, composition and size distributions (Seinfeld and Pandis, 2016). Although aerosol processes and properties are increasingly being treated in the global Earth System Models (ESMs) (Long et al., 2015;Tilmes et al., 2015) applied in the Coupled Model Intercomparison Project Phase 6 (CMIP-6) (Meehl et al., 2014), the scales on which such models are applied remain much coarser than those on which aerosol population properties are known to vary (Anderson et al., 2003). Therefore, limited area atmospheric models (regional models) applied at higher

resolution over specific regions of interest are expected to 'add value' (i.e. improve the fidelity) of the physical-dynamical-chemical processes that induce extreme events and dictate climate forcing. There is empirical evidence to suggest a strong resolution dependence in simulated aerosol particle properties. For example, WRF-Chem simulations with spatial resolution enhanced from 75 km to 3 km exhibited higher correlations and lower bias relative to observations of aerosol optical properties over Mexico likely due to more accurate description of emissions, meteorology and of the physicochemical processes that convert trace gases to particles (Gustafson et al., 2011;Qian et al., 2010). This improvement in the simulation of aerosol optical properties implies a reduction of the uncertainty in associated aerosol radiative forcing (Gustafson et al., 2011). Further, WRF-Chem run over the United Kingdom and Northern France at multiple resolutions in the range of 40-160 km, underestimated AOD by 10-16% and overestimated CCN by 18-36% relative to a high resolution run at 10 km, partly as a result of scale dependence of the gas-phase chemistry and differences in the aerosol uptake of water (Weigum et al., 2016).

However, debate remains regarding how to objectively evaluate model performance, quantify the value added by enhanced resolution (Di Luca et al., 2015;Rockel et al., 2008) and on possible limits to the improvement of climate representation in light of errors in the driving "imperfect lateral boundary conditions" (Diaconescu and Laprise, 2013). Nevertheless, although "it is unrealistic to expect a vast amount of added values since models already performs rather decently" (Di Luca et al., 2015) and global ESMs are now run at much higher resolution than in the past, it is generally assumed that high resolution regional models will add value via more realistic representation of spatio-temporal variability than global coarser-resolution simulations. Further, "the main added value of a regional climate model is provided by its small scales and its skill to simulate extreme events, particularly for precipitation" (Diaconescu and Laprise, 2013).

It is particularly challenging to assess the added-value from enhanced resolution in the context of climate-relevant aerosol properties since they are a complex product of the fidelity of the simulation of meteorological parameters, gas-phase precursors, emissions and the treatment of aerosol dynamics. Here we quantify the value added by enhanced resolution in the description of physical and chemical atmospheric conditions using year-long simulations from WRF-Chem over eastern North America, and investigate how they impact AOD. The primary performance evaluation of aerosol properties focuses on AOD at different wavelengths (λ = 470, 550 and 660 nm, where the AOD at different λ is used as a proxy of the aerosol size distribution (Tomasi

et al., 1983), see details in Sect. 2.3) and is measured relative to observations from satellite-borne instrumentation. Thus the term "value-added" is used here in the context of columnar aerosol properties to refer to an improvement of model performance in simulation of wavelength specific AOD as measured by the MODerate resolution Imaging Spectroradiometer (MODIS) instrument aboard the polar-orbiting Terra satellite. To attribute sources of the enhanced fidelity of AOD, our analysis also incorporates evaluation of the value-added by enhanced resolution in terms of key meteorological and gas-phase drivers of aerosol concentrations and composition and is conducted relative to the MERRA-2 reanalysis product for the physical variables and columnar gas concentrations from satellite observations (see details of the precise data sets used given below). The meteorological parameters considered are air temperature at 2 m (T_{2m}), total monthly precipitation (*PPT*), planetary boundary-layer height (*PBLH*) and specific humidity in the boundary layer (Q_{PBL}). The gas phase concentrations considered are sulfur dioxide (SO_2), ammonia (NH_3), nitrogen dioxide (NO_2) and formaldehyde (HCHO).

We begin by quantifying the performance of WRF-Chem when applied over eastern North America at a resolution of 60 km (WRF60) (~ finest resolution likely to be employed in CMIP-6 global simulations) and then compare the results to those from simulations conducted at 12 km (WRF12) (simulation details are given in Table 1). Quantification of model skill is undertaken by mapping the WRF12 output to the WRF60 grid (WRF12-remap) and computing Brier Skill Scores (BSS) using MODIS as the target, WRF60 as the reference forecast and WRF12-remap as the forecast to be evaluated. We also evaluate the performance of the WRF-Chem simulations of 2008 relative to climatology as represented by MODIS observations for 2000-2014. We additionally assess the impact of simulation resolution on extreme AOD values that are associated with enhanced impacts on climate and human health. This analysis uses both *Accuracy* and *Hit Rate* as the performance metrics and focuses on the co-occurrence of extreme values in space from the model output and MODIS.

Based on the performance evaluation of the WRF-Chem simulations that indicate substantial dry bias in the WRF60 simulations and large seasonality in the skill-scores for AOD as a function of resolution, we conducted two further year-long simulations at 60 km. In the first we held all other simulation conditions constant but selected a different cumulus parameterization. In the second, we held all simulation conditions constant but employed a different set of lateral boundary conditions for the meteorology. In the context of the precipitation biases reported herein it is worthy of note that discrepancies in simulated

precipitation regimes are key challenges in regional modelling (both physical and coupled with chemistry). Although the Grell 3D scheme has been successfully applied in a number of prior analysis wherein the model was applied at resolutions in the range of 1-36 km (e.g. (Grell and Dévényi, 2002;Lowrey and Yang, 2008;Nasrollahi et al., 2012;Sun et al., 2014;Zhang et al., 2016)), the North American Regional Climate Change Assessment Program (NARCCAP) simulations with WRF at 50-km were also dry biased in the study domain (Mearns et al., 2012). Although there have been a number of studies that have sought to evaluate different cumulus schemes over different regions at different resolutions, no definitive recommendation has been made regarding the dependence of model skill on resolution and cumulus parameterization (Arakawa, 2004;Jankov et al., 2005;Nasrollahi et al., 2012;Li et al., 2014). Hence, further research is needed to identify the optimal cumulus scheme for use over North America at coarser resolution. Thus, we performed a sensitivity analysis on the cumulus scheme at 60 km by applying the Grell-Freitas parameterization (Grell and Freitas, 2014), which is the next generation of the Grell 3D scheme.

2 Materials and Methods

2.1 WRF-Chem simulations

WRF-Chem (version 3.6.1) simulations were performed for the calendar year 2008 over eastern North America, in a domain centered over southern Indiana (86°W, 39°N) at two resolutions, one close to the finest resolution designed for CMIP-6 global model runs (i.e. 60 km, WRF60) and the other one at much higher resolution (12 km, WRF12). Simulation settings are identical for the two runs except for the time-step used for the physics (Table 1). Physical and chemical parameterizations were chosen to match previous work using WRF-Chem at 12 km on the same region which showed good performance relative to observations and the year 2008 was selected because it is representative of average climate and aerosol conditions during 2000 - 2014 (Crippa et al., 2016). More specifically the simulations adopted the RADM2 chemical mechanism (Stockwell et al., 1990) and a modal representation of the aerosol size distribution (MADE/SORGAM, (Ackermann et al., 1998;Schell et al., 2001)) with three lognormal modes and fixed geometric standard deviations (i.e. 1.7, 2 and 2.5 for Aitken, accumulation and coarse mode, respectively (Ackermann et al., 1998;Grell et al., 2005)). Aerosol direct feedback was turned on and coupled to the Goddard shortwave scheme (Fast et al., 2006). A telescoping vertical grid with 32 model layers from the surface to 50 hPa and 10 layers up to 800 hPa was selected. Meteorological initial and boundary conditions from the North American Mesoscale

Model at 12 km resolution (NAM12) are applied every 6 hours, while initial and chemical boundary conditions are taken from MOZART-4 (Model for Ozone and Related chemical Tracers, version 4) with meteorology from NCEP/NCAR-reanalysis (Emmons et al., 2010). Anthropogenic emissions are specified for both WRF60 and WRF12 from the US National Emission Inventory 2005 (NEI-05) (US-EPA, 2009) which provides hourly point and area emissions at 4 km on 19 vertical levels. The simulation settings and specifically the use of a modal representation of the aerosol size distribution were selected to retain computational tractability. Accordingly, the 60 km simulations for the year 2008 completed in 6.4 hours whereas the 12 km simulations completed in 9.5 days (230 hours) on the Cray XE6/XK7 supercomputer (Big Red II) owned by Indiana University, using 256 processors distributed on 8 nodes.

As described in detail below, in the WRF60 simulations configured as described in Table 1, simulated precipitation during the summer months exhibits substantial dry bias, and the analysis of value added by enhanced simulation resolution exhibited strong seasonality. We performed a sensitivity analysis to the cumulus scheme, by conducting an additional year-long simulation at 60 km using the Grell-Freitas parameterization (Grell and Freitas, 2014), which is an evolution of Grell 3D that is scale-aware and treats some aspects of aerosol-cloud interactions. We also tested the sensitivity of the simulation results to the meteorological boundary conditions, by repeating the WRF60 simulations using output from the Global Forecast System (GFS) at 0.5° resolution every 6 hours to provide the lateral boundary conditions.

2.2 Observations

Model aerosol optical properties are evaluated relative to the MODIS Collection 6 dark-target land aerosol product from aboard the Terra satellite (~1030 overpass local solar time (LST)) (Levy et al., 2013). To provide a consistent assessment of model skill, the evaluation of AOD is conducted only on land areas since the MODIS dark-target ocean aerosol product is based on a retrieval algorithm different from the one over land (Levy et al., 2013). Trace gas concentrations are evaluated relative to measurements from the Ozone Monitoring Instrument (OMI; version 3) (Chance, 2002) and the Infrared Atmospheric Sounding Interferometer (IASI; NN version 1) (Whitburn et al., 2016) aboard the Aura (~1345 LST) and MetOp satellites (~0930 LST), respectively. MODIS retrieves AOD at multiple λ including 470, 550, and 660 nm, and the MODIS algorithm removes cloud-contaminated pixels prior to spatial averaging

over 10 × 10 km (at nadir). OMI and IASI have nadir resolutions of 13 × 24 km and 12 km (circular footprint), respectively, and have been filtered to remove retrievals with cloud fractions > 0.3 (Fioletov et al., 2011;McLinden et al., 2014;Vinken et al., 2014) and OMI pixels affected by the row anomalies. MODIS, OMI, and IASI provide near daily global coverage, although the row anomalies render portions of the OMI viewing swath unusable. Uncertainty in AOD from MODIS is spatially and temporally variable. It has been estimated as ± (0.05 + 15%) for AOD over land (Levy et al., 2013), and prior research has reported 71% of MODIS Collection 5 retrievals fall within 0.05 ± 20% for AOD relative to AERONET in the study domain (Hyer et al., 2011). The accuracy of OMI ("root sum of the square of all errors, including forward model, inverse model, and instrument errors" (Brinksma et al., 2003)) is 1.1 DU or 50% for SO_2, 2×10^{14} cm^{-2}/30% for background/polluted NO_2 conditions, and 35% for HCHO. This uncertainty is typically reduced by spatial and temporal averaging, as employed herein (Fioletov et al., 2011;Krotkov et al., 2008). IASI NH_3 retrievals do not use an a priori assumption of emissions, vertical distribution, or lifetime of NH_3 (i.e. no averaging kernel); therefore, NH_3 accuracy is variable (Whitburn et al., 2016), and thus only retrievals with uncertainty lower than the retrieved concentrations are used herein.

For the model evaluation, satellite observations for each day are regridded to the WRF-Chem discretization. This is done by averaging all valid retrievals within: 0.1° and 0.35° of the WRF-Chem grid-cell center for the 12×12 km and 60×60 km resolutions, respectively for MODIS; 0.125° × 0.18° (along-track/latitudinal × cross-track/longitudinal) and 0.365° × 0.42° for OMI; 0.12° and 0.36° for IASI. To avoid issues from under-sampling, we require at least 10 valid MODIS granules for the 60×60 km daily average to be computed and at least 5 daily averages to compute a monthly average for each grid cell. Model evaluation of gaseous species is performed on a seasonal basis using standard scores (z-scores), which are computed as the difference between the seasonal mean within a grid cell and the seasonal spatial mean, divided by the seasonal spatial standard deviation. Use of z-scores allows comparison of the spatial patterns of satellite observations and model output in terms of standard deviation units from the mean.

The simulated meteorological properties are evaluated using Modern-Era Retrospective analysis for Research and Applications (MERRA-2) reanalysis data as the target. MERRA-2 is a homogenized and continuous in time description of atmospheric properties on a 3-dimensional global grid (horizontal resolution of 0.5°×0.625°, L72), developed by NASA and

was released in Fall 2015 (Molod et al., 2015). MERRA-2 provides hourly values of T_{2m} and *PBLH*, and vertical profile of 3-dimensional variables every 3 hours on a large number of pressure levels. Here we compute the total specific humidity (Q_{PBL}) of the lowest 8 pressure levels (i.e. in the boundary-layer approximated as the layer from 1000 to 825 hPa) in MERRA-2, assuming an average air density in the PBL of 1.1 kg m^{-3}. For the evaluation of simulated precipitation we use accumulated monthly total values.

2.3 Spectral dependence of AOD

Three properties dictate the actual aerosol direct radiative forcing: AOD, single scattering albedo and asymmetry factor, all of which are a function of the wavelength (λ) of incident radiation. The first property is related to the total columnar mass loading, typically dominates the variability of direct aerosol effect (Chin et al., 2009) and is the focus of the current research. The relationship between the aerosol size distribution and spectral dependence of AOD is described by a power law function:

$$b(l_1) = b(l_2) \times \left(\frac{l_1}{l_2}\right)^{-a} \quad \textbf{(1)}$$

where β is the particle extinction coefficient at a specific wavelength λ, and α is the Ångström exponent (Ångström, 1964) which describes the wavelength dependence of AOD (and is inversely proportional to the average aerosol diameter):

$$a = \frac{ln\frac{AOD(l_1)}{AOD(l_2)}}{ln\frac{l_2}{l_1}} \quad \textbf{(2)}$$

The aerosol volume distribution usually conforms to a multi-lognormal function with *n* modes:

$$\frac{dV(r)}{d\ln r} = \sum_{i=1}^{n} \frac{C_i}{\sqrt{2\pi}\sigma_i} \exp\left[\frac{-(\ln r - \ln R_i)^2}{2\sigma_i^2}\right] \quad \textbf{(3)}$$

where r is the particle radius and C_i, R_i and σ_i are the particle volume concentration, the geometric mean radius and the standard deviation in the mode i respectively.

We can thus compute AOD for a polydisperse distribution of aerosols with refractive index m in an atmospheric column of height Z as:

$$AOD(\lambda) = \int \frac{3\beta(m,r,\lambda)}{4r} \frac{dV(r)}{d\ln r} d\ln r dZ \quad \textbf{(4)}$$

As indicated in (Schuster et al., 2006), "the spectral variability of extinction diminishes for particles larger than the incident wavelength", thus fine mode particles contribute more to AOD in the visible (λ~0.5 μm) than at longer wavelengths, whereas coarse mode particles provide a similar AOD both at short and long wavelengths. This is reflected in the Ångström parameter which can be thus used as a proxy for the fine mode fraction or fine mode radius (Schuster et al., 2006).

2.4 Quantification of model performance and added-value

Taylor diagrams summarize three aspects of model performance relative to a reference: the spatial correlation coefficient (i.e. Pearson correlation of the fields, r), the ratio of spatial standard deviations of the two spatial fields ($\sigma_{wrf}/\sigma_{sat}$) and the root mean squared difference (RMSD) (Taylor, 2001). Here Taylor diagrams are presented for monthly mean AOD from WRF60, WRF12 and WRF12-remap relative to MODIS at different wavelengths (Fig. 1 d-f). Because AOD is not normally distributed, Spearman's rank correlation coefficients (ρ) of the mean monthly AOD spatial fields are also computed to reduce the impact of a few outliers and the small sample size during cold months (Table 2). To assess the significance of ρ while accounting for multiple testing, we apply a Bonferroni correction (Simes, 1986) in which for m hypothesis tests, the null hypothesis is rejected if $p \leq \frac{\alpha}{m}$, where p is the p-value and α is the confidence level (0.05 is used here).

We further quantify the value added (or lack of thereof) of the high-resolution simulations using the following metrics:

(i) Brier Skill Score

Value added is quantified using Brier Skill Scores (BSS) and is evaluated in two ways: first by evaluating the model performance as a function of simulation resolution and then using climatology as the reference 'forecast'. In these analyses the hourly output from the 12 km resolution simulation is degraded (averaged) to 60 km (hereafter WRF12-remap) as follows: the 12 km domain is resized excluding 2 grid cells at the border to exactly match the 60 km resolution domain. For example, in the analysis of AOD each coarse grid cell thus includes 5×5 12 km resolution cells and its value is the mean of all valid 12 km grid cells inside it if at least

half of those cells contain valid AOD (i.e. no cloud cover), otherwise the whole coarse cell is treated as missing. In all comparisons of AOD only cells with simultaneous (i.e. model and MODIS) clear sky conditions are considered. A daily value from WRF-Chem is computed as an instantaneous value for the hour nearest to the satellite overpass time. When the comparison is done on a monthly basis, a monthly mean value is computed from the daily values obtained under clear sky conditions, only if there are at least five valid observations in the month.

The primary metric used to quantify the added value of WRF12-remap versus WRF60 is the Brier Skill Score (BSS) (Murphy and Epstein, 1989):

$$BSS = \frac{r_{F'P'}^2 - \left(r_{F'P'} - \frac{\sigma_{F'}}{\sigma_{P'}} \right)^2 - \left(\frac{\langle P' \rangle - \langle F' \rangle}{\sigma_{P'}} \right)^2 + \left(\frac{\langle P' \rangle}{\sigma_{P'}} \right)^2}{1 + \left(\frac{\langle P' \rangle}{\sigma_{P'}} \right)^2} \quad \textbf{(5)}$$

where F is the "forecast" (i.e. the 12 km simulations mapped to 60 km, WRF12-remap); P is the "target" (i.e. for AOD this is MODIS at 60 km) and output from WRF60 are used as the reference forecast; F' the difference between 12 km estimates regridded to 60 km and MODIS; P' the difference between the 60 km simulation and the 'target' (i.e. for the AOD MODIS observations regridded to 60 km). In the analysis of BSS relative to the long-term (15-year) climatology of AOD from MODIS, the monthly mean climatological value of AOD is used as the reference forecast, while WRF60 and WRF12-remap are used as the forecasts, and monthly mean AOD from MODIS at 60 km is the target.

BSS measures by how much a test simulation (WRF12-remap) more closely (or poorly) reproduces observations (from MODIS, MERRA-2 or other satellite products) relative to a control (WRF60) run. For example, a BSS>0 indicates WRF12, even when regridded to 60 km, does add value. The first term in (5) ranges from 0 to 1, is described as the potential skill, and is the square of the spatial correlation coefficient between forecast and reference anomalies to MODIS. It is the skill score achievable if both the conditional bias (second term) and overall bias (third term) were zero, and for most of the variables considered herein (particularly AOD) it contributes to a positive BSS in most calendar months (and seasons). The second term (the conditional bias, > 0), is the square of the difference between the anomaly correlation coefficient and the ratio of standard deviation of the anomalies and is small if for all points F' is linear to P'. The third term is referred to as the forecast anomaly bias, and is the ratio of the difference between the mean anomalies of WRF12-remap and the observations relative to

315 WRF60 and the standard deviation of WRF60 anomaly relative to observed values. The fourth
316 term is the degree of agreement and appears in both the numerator and denominator. It is
317 computed as the square of the ratio of the mean anomaly between WRF60 and observations
318 and the standard deviation of the anomalies.

319 **(ii) Pooled paired t-test**

320 To identify which areas in space contribute most to the AOD added-value, we compare daily
321 mean AOD fields from WRF-Chem at different resolutions and MODIS. We perform a pooled
322 paired t-test to evaluate the null hypothesis that those differences come from normal
323 distributions with equal means and equal but unknown variances (the test statistic has a
324 Student's *t* distribution with df = n + m – 2, and the sample standard deviation is the pooled
325 standard deviation, where n and m are the two sample sizes). The test is conducted by
326 climatological season (e.g. winter = DJF) since there are fewer than 20 valid AOD observations
327 in most 60 km grid cells for each calendar month (Fig. 2). Given the large number of hypothesis
328 tests performed (i.e. one for each 60 km grid cell), we adjust the p-values using the False
329 Discovery Rate (FDR) approach (Benjamini and Hochberg, 1995). In this approach, p-values
330 from the t-tests are ranked from low to high ($p_1,p_2,\ldots,p_m$), then the test with the highest rank, *j*,
331 satisfying:

332 $$p_j \leq \frac{j}{m}\alpha \quad \textbf{(6)}$$

333 is identified. Here all p-values satisfying Eq. 6 with α=0.1 are considered significant.

334 **(iii) Accuracy and Hit Rate in identification of AOD extremes**

335 For each month we identify grid cells in which the wavelength specific AOD exceeds the 75th
336 percentile value computed from all grid cells and define that as an extreme. Thus grid cells
337 with extreme AOD are independently determined for MODIS and WRF-Chem at different
338 resolutions. The spatial coherence in identification of extremes in the fields is quantified using
339 two metrics: the *Accuracy* and the *Hit Rate* (*HR*). The *Accuracy* indicates the overall spatial
340 coherence and is computed as the number of grid cells co-identified as extreme and non-
341 extreme between WRF-Chem and MODIS relative to the total number of cells with valid data.
342 The *HR* weights only correct identification of extremes in MODIS by WRF-Chem.

343 **3 Results**

344 **3.1 Model performance as a function of spatial resolution**

When WRF-Chem is applied at 60 km resolution the degree of association of the resulting spatial fields of mean monthly AOD at the three wavelengths with MODIS varies seasonally. Smallest RMSD and highest Spearman spatial correlations (ρ) with MODIS observations generally occur during months with highest mean AOD (i.e. during summer, Fig. 1 d-f and Fig. 3), and reach a maximum in August ($\rho = 0.60$, Table 2). However, while the patterns of relative AOD variability are well captured, the absolute magnitudes and spatial gradients of AOD during the summer are underestimated by WRF60 (Fig. 1 d-f and Fig. 3, Table S1). High spatial correlations ($\rho > 0.40$) are also observed in March, April and November (Table 2), when the ratio of spatial standard deviations is closer to 1 (Fig. 1 d-f, Table S1). Only a weak wavelength dependence is observed in the performance metrics as described on Taylor diagrams. The spatial variability is generally more negatively biased for AOD at 660 nm (Table S1), indicating that WRF60 simulations tend to produce larger diameter aerosols homogeneously distributed over the domain, whereas MODIS observations indicate more spatial variability.

The performance of WRF60 simulations relative to MODIS contrasts with analyses of WRF12 and WRF12-remap. WRF12 and WRF12-remap indicate highest spatial correlations with MODIS observations throughout the summer months ($\rho = 0.5$-0.7, Table 2), although the bias towards simulation of more coarse aerosols than are observed is consistent across the two simulations and with prior research (see details provided in (Crippa et al., 2016)). However, simulations at 12 km (WRF12) show positive ρ with MODIS for all λ in all calendar months, while mean monthly spatial fields of AOD from WRF60 show low and/or negative correlations with MODIS during May, June, September, October and December, indicating substantial differences in the degree of correspondence with MODIS AOD in the two simulations, and higher fidelity of the enhanced resolution runs (Tables 2 and S1).

Monthly mean spatial fields of AOD(λ) as simulated by WRF12 or WRF12-remap exhibit positive Spearman correlation coefficients (ρ) with MODIS observations for all calendar months and range from ~ 0.25 for WRF12-remap (0.20 for WRF12) during winter to ~ 0.70 and 0.64, respectively during summer (Table 2). Spearman's ρ are uniformly higher in WRF12-remap than WRF12 indicating a mismatch in space in the high-resolution simulation (i.e. that grid cells with high AOD are slightly displaced in the 12 km simulations possibly due to the presence of sub-grid scale aerosol plumes (Rissman et al., 2013)). Mean monthly fields of AOD (all λ) from both WRF12 and WRF12-remap exhibit lower ρ with MODIS in February-April and November than the 60 km runs (Table 2). These discrepancies appear to be driven by

conditions in the south of the domain. For example, differences between WRF60/WRF12-remap vs. MODIS during all seasons are significant according to the paired t-test over Florida and along most of the southern coastlines (Fig. 2). This region of significant differences extends up to ~ 40°N during summer and fall, reflecting the stronger north-south gradient in AOD from MODIS and WRF12-remap that is not captured by WRF60 (see example for λ = 550 nm, Fig. 3). These enhancements in the latitudinal gradients from WRF12-remap are also manifest in the physical variables (particularly specific humidity as discussed further below).

The differences in the absolute values of mean monthly AOD deriving from differences in the resolution at which WRF-Chem was applied are of sufficient magnitude (a difference of up to 0.2 in regions with a mean AOD value of 0.4), particularly in the summer months (Fig. 4), to raise concerns. However, detailed investigation of the simulations settings and repetition of the 60 km simulation resulted in virtually identical results indicating no fault can be found in the analysis. Further, we note that the eastern-half of North America was also identified as a region of high discrepancy in global ESM (Myhre et al., 2013a).

To further investigate differences in the simulation output due to spatial discretization we computed Brier Skill Scores (BSS). In this analysis AOD for each λ from WRF12-remap are used as the 'forecast', output from WRF60 are used as the reference forecast and MODIS observations at 60 km are used as the target. BSS exceed 0 during all months except for September and October, and largest BSS (> 0.5) for AOD (all λ) is found during most months between December and July (Fig. 5a-c). This indicates that running WRF-Chem at 12 km resolution yields higher skill in simulated AOD relative to WRF60, even when the WRF12 output is remapped to 60 km. BSS do not strongly depend on λ, indicating the added value from enhanced resolution similarly affects aerosol particles of different sizes. Inspecting the terms defining the BSS provides information about the origin of the added value (Fig. 5a-c). The positive BSS derives principally from the potential skill (first term in Eq. 5), which demonstrates a reduction in bias and/or more accurate representation of the spatial gradients in WRF12-remap. This term exhibits weak seasonality with values below 0.5 only during August and fall months. The second and third terms are close to zero during most months, although bigger biases are found during August-October. The substantial conditional bias during late summer and early fall is the result of the large ratio of standard deviations (> 1, i.e. the spatial variability of the anomaly relative to MODIS is larger for WRF12-remap than WRF60, Table S1). It thus contributes to the negative BSS found in September and October, which are also identified as outlier months in WRF12-remap from the Taylor diagram analysis (Fig. 1). Output

for these months show modest spatial correlations with AOD from MODIS and higher ratio of standard deviations than in WRF60-MODIS comparisons (Fig. 1, Table S1). Previous work showed that the lower model skill (in WRF12) during September and October may be partially attributable to a dry bias in precipitation from WRF-Chem relative to observations. As a result, simulated AOD and near-surface aerosol nitrate and sulfate concentrations are positively biased over large parts of the domain (Crippa et al., 2016). Although the effects of the boundary conditions appear in some variables (e.g. in Fig. 4 and Figs. S1-S3), the BSS results do not significantly change even when those cells are removed from the analysis.

When the BSS is used to assess the skill of each model relative to MODIS AOD climatological mean over the years 2000-2014, WRF12-remap is found to add value relative to the climatology (i.e. BSS >0) during summer months and Nov-Jan whereas BSS for WRF60 is positive from late Fall to early Spring (Fig. 5d). The fact that WRF-Chem does not always outperform the climatology is expected since the model is based on time invariant emissions and skill is assessed relative to a year selected to be representative of the AOD climatology. Mean seasonal AOD from MODIS retrievals over the study region during 2008 lie within ±0.2 standard deviations of the climatology (Crippa et al., 2016). Interestingly, BSS for most months (excluding September) are higher for the WRF60 simulations conducted using lateral boundary conditions from NAM12 than GFS.

Model resolution also affects the *Accuracy* and *Hit Rate* (*HR*) for identification of areas of extreme AOD (AOD>75th percentile). Highest coherence in the identification of extreme AOD in space identified in WRF12-remap (and WRF12) relative to MODIS is found during May-August (*HR* = 53-77%) vs. WRF60 (*HR* = 17-54%, Table 3). Conversely highest *HR* are found for WRF60 and MODIS during winter and early spring, and indeed exceed those for WRF12 and WRF12-remap (Table 3, e.g. Feb: *HR* = 0.78 for WRF60, and 0.67 and 0.68 for WRF12 and WRF12-remap, respectively). These differences are consistent with the observation that WRF12-remap overestimates the scales of AOD coherence and AOD magnitude during the cold season along coastlines and over much of the domain in April (Fig. 3).

The synthesis of these analyses is thus that the higher resolution simulation increases the overall spatial correlation, decreases overall bias in AOD close to the peak of the solar spectrum relative to MODIS observations and therefore the higher-resolution simulations better represent aerosol direct climate forcing. However, WRF12-remap exhibits little improvement over WRF60 in terms of reproducing the spatial variability of AOD in the visible wavelengths and further that WRF12-remap tends to be more strongly positively biased in terms of mean

monthly AOD outside of the summer months (Fig. 2 and Fig. 3). Also the improvement in detection of areas of extreme AOD in the higher resolution simulations (WRF12-remap) is manifest only during the warm season.

3.2 Investigating sources of error in simulated AOD

As documented above, WRF-Chem applied at either 60 or 12 km resolution over eastern North America exhibits some skill in reproducing observed spatial fields of AOD and the occurrence of extreme AOD values. However, marked discrepancies both in space and time are found, and at least some of them show a significant dependence on model resolution. Thus, we investigated a range of physical conditions and gas phase concentrations known to be strongly determinant of aerosol dynamics in terms of the BSS as a function of model resolution and also in terms of the mean monthly spatial patterns.

WRF12 even when remapped to 60 km provides more accurate description of key meteorological variables such as specific humidity (*Q*) within the boundary layer, *PBLH*, surface temperature and precipitation (see Fig. 6, S1, S2 and S3) when compared to MERRA-2, as indicated by the positive BSS during almost all months (Fig. 7a). Good qualitative agreement is observed for the spatial patterns and absolute magnitude of T_{2m} in both WRF60 and WRF12-remap relative to MERRA-2 for all seasons (Fig. S1) leading to only modest magnitude of BSS (i.e. value added by the higher resolution simulations (Fig. 7a)). The aerosol size distribution and therefore wavelength specific AOD exhibits a strong sensitivity to *Q* (Santarpia et al., 2005) due to the presence of hygroscopic components in atmospheric aerosols and thus the role of water uptake in determining aerosol diameter, refractivity and extinction coefficient (Zieger et al., 2013). For example, the hygroscopic growth factor, which indicates the change of aerosol diameter due to water uptake, is ~ 1.4 for pure ammonium sulfate with dry diameter of 532 nm at relative humidity of 80%, thus biases in representation atmospheric humidity may lead to big errors in simulated aerosol size and AOD (Flores et al., 2012). Our previous analyses of the 12 km resolution simulations indicated overestimation of sulfate aerosols (a highly hygroscopic aerosol component, and one which in many chemical forms exhibits strong hysteresis (Martin et al., 2004)) relative to observed near-surface $PM_{2.5}$ concentrations during all seasons except for winter (Crippa et al., 2016), leading to the hypothesis that simulated AOD and discrepancies therein may exhibit a strong dependence on *Q*. Consistent with that postulate, Q_{PBL} from WRF12-remap exhibits a moist bias in cloud-free grid cells mostly during warm months, whereas WRF60 is characterized by a dry bias during all seasons (Fig. 6). Despite the positive bias, WRF12-remap better captures the seasonal

spatial patterns of Q_{PBL} in MERRA-2, leading to positive BSS for this variable in all calendar months. Thus, there is added value by higher-resolution simulations in representation of one of the key parameters dictating aerosol particle growth and optical properties. Spatial patterns of differences in Q_{PBL} from WRF60 and WRF12-remap relative to MERRA-2 (Fig. 6) exhibit similarities to differences in AOD (Fig. 4). WRF60 is dry-biased relative to WRF12 particularly during the summer (and fall) and underestimates Q_{PBL} relative to MERRA-2 during all seasons over the southern states and over most of continental US during summer and fall. Conversely, WRF12-remap overestimates Q_{PBL} over most of continental US during summer and fall relative to MERRA-2.

PBLH is a key variable for dictating near-surface aerosol concentrations but is highly sensitive to the physical schemes applied, and biases appear to be domain and resolution dependent. However, this parameter is comparatively difficult to assess because differences in *PBLH* from WRF-Chem and MERRA-2 may also originate from the way they are computed (i.e. from heat diffusivity in MERRA-2 (Jordan et al., 2010) and from turbulent kinetic energy in WRF-Chem (Janjić, 2002;von Engeln and Teixeira, 2013)). Nevertheless, the Mellor-Yamada-Janjich *PBL* scheme combined with the Noah Land Surface Model applied in this work was found to produce lower *PBL* heights (Zhang et al., 2009) than other parameterizations. Thus, the positive bias in simulated AOD and surface $PM_{2.5}$ concentrations (reported previously in (Crippa et al., 2016)) may be linked to the systematic underestimation of *PBLH* simulated by WRF12-remap over continental US relative to MERRA-2 during all seasons (except winter) with greatest bias over regions of complex topography (Fig. S2). A positive bias (of several hundred meters) in terms of *PBLH* for WRF simulations using the MYJ parameterization was previously reported for high-resolution simulations over complex terrain (Rissman et al., 2013), and a positive bias in *PBLH* is also observed in the 60 km simulations presented herein (Fig. S2). This may provide a partial explanation for the large negative bias in AOD in WRF60 during summer (Fig. 3). In general, the BSS indicate improvement in the simulation of *PBLH* in WRF12-remap than in WRF60 (Fig. 7a).

Consistent with the dry bias in Q_{PBL} in WRF60, total accumulated precipitation is also underestimated in WRF60, while WRF12-remap captures the absolute magnitudes and the spatial patterns therein (Fig. S3). Analyses of hourly precipitation rates also show higher skill for WRF12-remap than WRF60 in simulating precipitation occurrence (*HR*) relative to MERRA-2 (Table S2). More specifically WRF12-remap correctly predicts between 40% and 70 % of precipitation events in MERRA-2 with highest skill during winter months, whereas

WRF60 output exhibits lower HR (~6% during summer and 30% during winter). This result thus confirms our expectation of a strong sensitivity of model performance to resolution due to the inherent scale dependence in the cumulus scheme. Use of the Grell-Freitas parameterization in the WRF60 simulations did not lead to substantially different magnitude and/or spatial patterns of precipitation compared to WRF60 applied with the Grell 3D scheme, and no improvement in agreement with output from MERRA2. The findings of a negative bias in precipitation amounts in WRF60 simulations without a corresponding overestimation of AOD may appear counter-intuitive since aerosol concentrations (and thus AOD) are dependent on aerosol residence times and analyses of sixteen global models from the AeroCom project indicate wet scavenging is the dominant removal process for most aerosol species in the study area (Hand et al., 2012;Textor et al., 2006). However, the negative precipitation bias in WRF60 simulations appears to also be linked to poor representation of surface moisture availability, boundary layer humidity (Fig. 6), and ultimately aerosol water content (and hence AOD).

Gas phase concentrations (transformed into z-scores) from WRF12-remap show higher agreement with satellite observations during almost all months, as indicated by the positive BSS (Fig. 7b). However given the limited availability of valid satellite observations (especially during months with low radiation intensity), the BSS are likely only robust for the summer months for all species. Nevertheless, with the exception of NH_3 during June, BSS for all months are above or close to zero indicating that on average, the enhanced resolution simulations do exhibit higher skill in the simulation of the gas phase species even when remapped to 60 km resolution. Further, the seasonal average spatial patterns of the total columnar concentrations, expressed in terms of z-scores, also exhibit qualitative agreement with the satellite observations (Fig. S4-S7).

4 Concluding remarks

This analysis is one of the first to quantify the impact of model spatial resolution on the spatio-temporal variability and magnitude of meteorological and chemical parameters and how representation of these variables impact AOD, and does so using simulations for a full calendar year. Application of WRF-Chem at two different resolutions (60 km and 12 km) over eastern North America for a representative year (2008) leads to the following conclusions:

- Higher-resolution simulations improve the representation of key meteorological variables such as temperature, near-surface specific humidity, boundary layer height and the occurrence and amount of precipitation. Both spatial patterns and precipitation

occurrence are better captured by WRF12-remap, and particularly during the summer months the specific humidity within the boundary-layer exhibits closer agreement with a reanalysis product when WRF is applied at higher resolution. The dry bias in the low-resolution WRF-Chem simulations (60 km) is consistent with previous research over eastern North America, and is manifest in simulations with two different cumulus parameterizations and two different data sets for the LBC (GFS and NAM12).

- More accurate representation of spatial patterns and concentration of gaseous species that either play a key role in particle formation and growth or are indicators of primary aerosol emissions is also achieved by running WRF-Chem at high resolution.
- Partly/largely due to the improved fidelity of key meteorological parameters and gas-phase aerosol precursor species, higher resolution simulations enhance the fidelity of AOD representation at and near to the peak in the solar spectrum relative to a coarser run. At least some of the improvement in the accuracy with which AOD is reproduced in the higher resolution simulations may be due to improved fidelity of specific humidity and thus more accurate representation of hygroscopic growth of some aerosol components. Spatial correlations of AOD from WRF12 and WRF12-remap with observations from MODIS are higher than AOD from a simulation conducted at 60 km during most months. WRF12 show positive spatial correlations with MODIS for all λ in all calendar months, and particularly during summer (ρ = 0.5-0.7). However, the improvement in model performance is not uniform in space and time.
- Output from WRF12 and WRF12-remap exhibit highest accord with MODIS observations in capturing the frequency, magnitude and location of extreme AOD values during summer when AOD is typically highest. During May-August WRF12-remap has *Hit Rates* for identification of extreme AOD of 53-78%.

It is worthy of note that even the 12 km resolution WRF-Chem simulations exhibit substantial differences in AOD relative to MODIS over eastern North America, and the agreement varies only slightly with wavelength. This may be partially attributable to use of the modal approach to represent the aerosol size distribution in order to enhance computational tractability. In this application each mode has a fixed geometric standard deviation (σ_g), which can lead to biases in simulated AOD in the visible wavelengths by up to 25% (Brock et al., 2016) (with the model overestimating observations if the prescribed σ_g is larger than the observed one). Setting σ_g = 2 for the accumulation mode (the default in WRF-Chem) may lead to an overestimation of the number of particles at the end of the accumulation mode tail, and there is evidence that a value

of $\sigma_{g,acc}$=1.40 leads to higher agreement with observations (Mann et al., 2012). Further possible sources of the AOD biases reported herein derive from selection of the physical schemes (e.g. planetary boundary layer (*PBL*) schemes and land-surface model (Misenis and Zhang, 2010;Zhang et al., 2009)). Further, it is worth mentioning that NEI emissions are specified based on an average summertime weekday, so enhanced model performance might be achieved if seasonally varying emissions were available.

Naturally, there is a need for more research regarding the sensitivity of WRF-Chem simulations of climate relevant aerosol properties to the parameterizations used, the lateral boundary conditions employed and the resolution at which the simulations are conducted. Further, attribution of added-value in the simulation of AOD by enhanced spatial resolution is necessary and will be facilitated by identifying simulation settings that minimize bias in the variables affecting AOD. This research will be part of future investigations.

Acknowledgments

This research was supported in part by a L'Oréal-UNESCO UK and Ireland Fellowship For Women In Science (to PC), the Natural Environmental Research Council (NERC) through the LICS project (ref. NE/K010794/1), grants to SCP from US NSF (grant # 1517365) and NASA (NNX16AG31G), and a NASA Earth and Space Science Fellowship Program - Grant "14-EARTH14F-0207" (to RCS). Further support was provided by the Lilly Endowment, Inc., through its support for the Indiana University Pervasive Technology Institute and the Indiana METACyt Initiative. We gratefully acknowledge the NASA scientists responsible for MERRA-2 and MODIS products, the developers of WRF-Chem, and Lieven Clarisse, Simon Whitburn, and Martin Van Damme for producing and sharing the NH_3 retrievals. The clarity and content of this manuscript was substantially improved by the comments of three reviewers.

References

Ackermann, I. J., Hass, H., Memmesheimer, M., Ebel, A., Binkowski, F. S., and Shankar, U.: Modal aerosol dynamics model for Europe: development and first applications, Atmospheric Environment, 32, 2981-2999, http://dx.doi.org/10.1016/S1352-2310(98)00006-5, 1998.

Anderson, T. L., Charlson, R. J., Winker, D. M., Ogren, J. A., and Holmén, K.: Mesoscale Variations of Tropospheric Aerosols, Journal of the Atmospheric Sciences, 60, 119-136, doi: http://dx.doi.org/10.1175/1520-0469(2003)060<0119:MVOTA>2.0.CO;2, 2003.

Ångström, A.: The parameters of atmospheric turbidity, Tellus, 16, 64-75, 10.1111/j.2153-3490.1964.tb00144.x, 1964.

606 Arakawa, A.: The Cumulus Parameterization Problem: Past, Present, and Future, Journal of
607 Climate, 17, 2493-2525, doi:10.1175/1520-0442(2004)017<2493:RATCPP>2.0.CO;2, 2004.

608 Benjamini, Y., and Hochberg, Y.: Controlling the False Discovery Rate: A Practical and
609 Powerful Approach to Multiple Testing, Journal of the Royal Statistical Society. Series B
610 (Methodological), 57, 289-300, 1995.

611 Boucher, O., D. Randall, P. Artaxo, C. Bretherton, G. Feingold, P. Forster, V.-M. Kerminen,
612 Y. Kondo, H. Liao, U. Lohmann, P. Rasch, S.K. Satheesh, S. Sherwood, B. Stevens and X.Y.
613 Zhang: Clouds and Aerosols, in: Climate Change 2013: The Physical Science Basis.
614 Contribution of Working Group I to the Fifth Assessment Report of the Intergovernmental
615 Panel on Climate Change, edited by: Stocker, T. F., D. Qin, G.-K. Plattner, M. Tignor, S.K.
616 Allen, J. Boschung, A. Nauels, Y. Xia, V. Bex and P.M. Midgley, Cambridge University Press,
617 Cambridge, United Kingdom and New York, NY, USA, 33–115, 2013.

618 Brinksma, E. J., Boersma, K. F., Levelt, P. F., and McPeters, R. D.: OMI validation
619 requirements document, Version 1, Rep. RS-OMIE-KNMI-345, 66, 2003.

620 Brock, C. A., Wagner, N. L., Anderson, B. E., Attwood, A. R., Beyersdorf, A., Campuzano-
621 Jost, P., Carlton, A. G., Day, D. A., Diskin, G. S., Gordon, T. D., Jimenez, J. L., Lack, D. A.,
622 Liao, J., Markovic, M. Z., Middlebrook, A. M., Ng, N. L., Perring, A. E., Richardson, M. S.,
623 Schwarz, J. P., Washenfelder, R. A., Welti, A., Xu, L., Ziemba, L. D., and Murphy, D. M.:
624 Aerosol optical properties in the southeastern United States in summer – Part 1: Hygroscopic
625 growth, Atmospheric Chemistry and Physics, 16, 25695-25738, doi:10.5194/acp-16-5009-
626 2016, 2016.

627 Chance, K.: OMI algorithm theoretical basis document, volume IV: OMI trace gas algorithms,
628 2002.

629 Chen, F., and Dudhia, J.: Coupling an advanced land surface–hydrology model with the Penn
630 State–NCAR MM5 modeling system. Part I: model implementation and sensitivity, Monthly
631 Weather Review, 129, 569-585, doi:10.1175/1520-
632 0493(2001)129<0569:CAALSH>2.0.CO;2, 2001.

633 Chin, M., Kahn, R. A., and Schwartz , S. E.: Atmospheric Aerosols Properties and Climate
634 Impacts. A Report by the U.S. Climate Change Science Program and the Subcommittee on
635 Global Change Research, in, National Aeronautics and Space Administration, Washington,
636 D.C., USA, 128, 2009.

637 Crippa, P., Sullivan, R. C., Thota, A., and Pryor, S. C.: Evaluating the skill of high-resolution
638 WRF-Chem simulations in describing drivers of aerosol direct climate forcing on the regional
639 scale, Atmospheric Chemistry and Physics, 16, 397-416, 10.5194/acp-16-397-2016, 2016.

640 Di Luca, A., de Elía, R., and Laprise, R.: Challenges in the Quest for Added Value of Regional
641 Climate Dynamical Downscaling, Curr Clim Change Rep, 1, 10-21, 10.1007/s40641-015-
642 0003-9, 2015.

643 Diaconescu, E., and Laprise, R.: Can added value be expected in RCM-simulated large scales?,
644 Climate Dynamics, 41, 1769-1800, 10.1007/s00382-012-1649-9, 2013.

Emmons, L. K., Walters, S., Hess, P. G., Lamarque, J. F., Pfister, G. G., Fillmore, D., Granier, C., Guenther, A., Kinnison, D., Laepple, T., Orlando, J., Tie, X., Tyndall, G., Wiedinmyer, C., Baughcum, S. L., and Kloster, S.: Description and evaluation of the Model for Ozone and Related chemical Tracers, version 4 (MOZART-4), Geoscientific Model Development, 3, 43-67, doi:10.5194/gmd-3-43-2010, 2010.

Fast, J. D., Gustafson, W. I., Easter, R. C., Zaveri, R. A., Barnard, J. C., Chapman, E. G., Grell, G. A., and Peckham, S. E.: Evolution of ozone, particulates, and aerosol direct radiative forcing in the vicinity of Houston using a fully coupled meteorology-chemistry-aerosol model, Journal of Geophysical Research: Atmospheres, 111, D21305, 10.1029/2005JD006721, 2006.

Fioletov, V. E., McLinden, C. A., Krotkov, N., Moran, M. D., and Yang, K.: Estimation of SO_2 emissions using OMI retrievals, Geophysical Research Letters, 38, L21811, 10.1029/2011GL049402, 2011.

Flores, J. M., Bar-Or, R. Z., Bluvshtein, N., Abo-Riziq, A., Kostinski, A., Borrmann, S., Koren, I., Koren, I., and Rudich, Y.: Absorbing aerosols at high relative humidity: linking hygroscopic growth to optical properties, Atmospheric Chemistry and Physics, 12, 5511-5521, 10.5194/acp-12-5511-2012, 2012.

Grell, G. A., and Dévényi, D.: A generalized approach to parameterizing convection combining ensemble and data assimilation techniques, Geophysical Research Letters, 29, 38-31-38-34, 10.1029/2002GL015311, 2002.

Grell, G. A., Peckham, S. E., Schmitz, R., McKeen, S. A., Frost, G., Skamarock, W. C., and Eder, B.: Fully coupled "online" chemistry within the WRF model, Atmospheric Environment, 39, 6957-6975, 10.1016/j.atmosenv.2005.04.027, 2005.

Grell, G. A., and Freitas, S. R.: A scale and aerosol aware stochastic convective parameterization for weather and air quality modeling, Atmospheric Chemistry and Physics, 14, 5233-5250, 10.5194/acp-14-5233-2014, 2014.

Guenther, A., Zimmerman, P., and Wildermuth, M.: Natural volatile organic compound emission rate estimates for U.S. woodland landscapes, Atmospheric Environment, 28, 1197-1210, 10.1016/1352-2310(94)90297-6, 1994.

Guenther, A. B., Zimmerman, P. R., Harley, P. C., Monson, R. K., and Fall, R.: Isoprene and monoterpene emission rate variability: model evaluations and sensitivity analyses, J. Geophys. Res.-Atmos., 98, 12609-12617, 10.1029/93jd00527, 1993.

Gustafson, W. I., Qian, Y., and Fast, J. D.: Downscaling aerosols and the impact of neglected subgrid processes on direct aerosol radiative forcing for a representative global climate model grid spacing, Journal of Geophysical Research: Atmospheres, 116, D13303, 10.1029/2010JD015480, 2011.

Hand, J. L., Schichtel, B. A., Pitchford, M., Malm, W. C., and Frank, N. H.: Seasonal composition of remote and urban fine particulate matter in the United States, J. Geophys. Res.-Atmos., 117, 10.1029/2011jd017122, 2012.

683 Hong, S.-Y., Dudhia, J., and Chen, S.-H.: A Revised Approach to Ice Microphysical Processes
684 for the Bulk Parameterization of Clouds and Precipitation, Monthly Weather Review, 132, 103-
685 120, doi:10.1175/1520-0493(2004)132<0103:ARATIM>2.0.CO;2, 2004.

686 Hyer, E. J., Reid, J. S., and Zhang, J.: An over-land aerosol optical depth data set for data
687 assimilation by filtering, correction, and aggregation of MODIS Collection 5 optical depth
688 retrievals, Atmospheric Measurement Techniques, 4, 379-408, 10.5194/amt-4-379-2011,
689 2011.

690 Janjić, Z. I.: The Step-Mountain Eta Coordinate Model: Further Developments of the
691 Convection, Viscous Sublayer, and Turbulence Closure Schemes, Monthly Weather Review,
692 122, 927-945, doi:10.1175/1520-0493(1994)122<0927:TSMECM>2.0.CO;2, 1994.

693 Janjić, Z. I.: Nonsingular implementation of the Mellor–Yamada level 2.5 scheme in the NCEP
694 Meso model, NCEP office note, 437, 61, 2002.

695 Jankov, I., A. Gallus, J. W., Segal, M., Shaw, B., and E. Koch, S.: The Impact of Different
696 WRF Model Physical Parameterizations and Their Interactions on Warm Season MCS
697 Rainfall, Weather and Forecasting, 20, 1048-1060, doi:10.1175/WAF888.1, 2005.

698 Jordan, N. S., Hoff, R. M., and Bacmeister, J. T.: Validation of Goddard Earth Observing
699 System-version 5 MERRA planetary boundary layer heights using CALIPSO, J. Geophys.
700 Res.-Atmos., 115, 10.1029/2009jd013777, 2010.

701 Krotkov, N. A., McClure, B., Dickerson, R. R., Carn, S. A., Li, C., Bhartia, P. K., Yang, K.,
702 Krueger, A. J., Li, Z., Levelt, P. F., Chen, H., Wang, P., and Lu, D.: Validation of SO_2 retrievals
703 from the Ozone Monitoring Instrument over NE China, Journal of Geophysical Research:
704 Atmospheres, 113, D16S40, 10.1029/2007JD008818, 2008.

705 Leibensperger, E., Mickley, L. J., Jacob, D. J., Chen, W.-T., Seinfeld, J., Nenes, A., Adams,
706 P., Streets, D., Kumar, N., and Rind, D.: Climatic effects of 1950–2050 changes in US
707 anthropogenic aerosols–Part 1: Aerosol trends and radiative forcing, Atmospheric Chemistry
708 and Physics, 12, 3333-3348, doi:10.5194/acp-12-3333-2012, 2012.

709 Levy, R. C., Mattoo, S., Munchak, L. A., Remer, L. A., Sayer, A. M., Patadia, F., and Hsu, N.
710 C.: The Collection 6 MODIS aerosol products over land and ocean, Atmospheric Measurement
711 Techniques, 6, 2989-3034, 10.5194/amt-6-2989-2013, 2013.

712 Li, L. F., Li, W. H., and Jin, J. M.: Improvements in WRF simulation skills of southeastern
713 United States summer rainfall: physical parameterization and horizontal resolution, Climate
714 Dynamics, 43, 2077-2091, 10.1007/s00382-013-2031-2, 2014.

715 Long, M., Yantosca, R., Nielsen, J., Keller, C., da Silva, A., Sulprizio, M., Pawson, S., and
716 Jacob, D.: Development of a grid-independent GEOS-Chem chemical transport model (v9-02)
717 as an atmospheric chemistry module for Earth system models, Geoscientific Model
718 Development, 8, 595-602, doi:10.5194/gmd-8-595-2015, 2015.

719 Lowrey, M. R. K., and Yang, Z. L.: Assessing the Capability of a Regional-Scale Weather
720 Model to Simulate Extreme Precipitation Patterns and Flooding in Central Texas, Weather and
721 Forecasting, 23, 1102-1126, 10.1175/2008waf2006082.1, 2008.

Mann, G. W., Carslaw, K. S., Ridley, D. A., Spracklen, D. V., Pringle, K. J., Merikanto, J., Korhonen, H., Schwarz, J. P., Lee, L. A., Manktelow, P. T., Woodhouse, M. T., Schmidt, A., Breider, T. J., Emmerson, K. M., Reddington, C. L., Chipperfield, M. P., and Pickering, S. J.: Intercomparison of modal and sectional aerosol microphysics representations within the same 3-D global chemical transport model, Atmospheric Chemistry and Physics, 12, 4449-4476, 10.5194/acp-12-4449-2012, 2012.

Martin, S. T., Hung, H. M., Park, R. J., Jacob, D. J., Spurr, R. J. D., Chance, K. V., and Chin, M.: Effects of the physical state of tropospheric ammonium-sulfate-nitrate particles on global aerosol direct radiative forcing, Atmospheric Chemistry and Physics, 4, 183-214, doi:10.5194/acp-4-183-2004, 2004.

McComiskey, A., Schwartz, S. E., Schmid, B., Guan, H., Lewis, E. R., Ricchiazzi, P., and Ogren, J. A.: Direct aerosol forcing: Calculation from observables and sensitivities to inputs, Journal of Geophysical Research: Atmospheres, 113, D09202, 10.1029/2007JD009170, 2008.

McLinden, C. A., Fioletov, V., Boersma, K. F., Kharol, S. K., Krotkov, N., Lamsal, L., Makar, P. A., Martin, R. V., Veefkind, J. P., and Yang, K.: Improved satellite retrievals of NO_2 and SO_2 over the Canadian oil sands and comparisons with surface measurements, Atmospheric Chemistry and Physics, 14, 3637-3656, 10.5194/acp-14-3637-2014, 2014.

Mearns, L. O., Arritt, R., Biner, S., Bukovsky, M., Stain, S., and NARCCAP team The North American Regional Climate Change Assessment Program: Overview of Phase I Results, Bulletin of the American Meteorological Society, 93, 1337-1362, 2012.

Meehl, G. A., Moss, R., Taylor, K. A., Eyring, V., Stouffer, R. J., Sandrine, B., and Stevens, B.: Climate model intercomparisons: preparing for the next phase, Eos, Transaction, American Geophysical Union, 95, 77-84, doi:10.1002/2014EO09, 2014.

Misenis, C., and Zhang, Y.: An examination of sensitivity of WRF/Chem predictions to physical parameterizations, horizontal grid spacing, and nesting options, Atmospheric Research, 97, 315-334, 10.1016/j.atmosres.2010.04.005, 2010.

Mlawer, E. J., Taubman, S. J., Brown, P. D., Iacono, M. J., and Clough, S. A.: Radiative transfer for inhomogeneous atmospheres: RRTM, a validated correlated-k model for the longwave, Journal of Geophysical Research: Atmospheres, 102, 16663-16682, 10.1029/97JD00237, 1997.

Molod, A., Takacs, L., Suarez, M., and Bacmeister, J.: Development of the GEOS-5 atmospheric general circulation model: evolution from MERRA to MERRA2, Geoscientific Model Development, 8, 1339-1356, 10.5194/gmd-8-1339-2015, 2015.

Murphy, A. H., and Epstein, E. S.: Skill scores and correlation-coefficients in model verification, Monthly Weather Review, 117, 572-581, 10.1175/1520-0493(1989)117<0572:ssacci>2.0.co;2, 1989.

Myhre, G., Samset, B. H., Schulz, M., Balkanski, Y., Bauer, S., Berntsen, T. K., Bian, H., Bellouin, N., Chin, M., Diehl, T., Easter, R. C., Feichter, J., Ghan, S. J., Hauglustaine, D., Iversen, T., Kinne, S., Kirkevag, A., Lamarque, J. F., Lin, G., Liu, X., Lund, M. T., Luo, G., Ma, X., van Noije, T., Penner, J. E., Rasch, P. J., Ruiz, A., Seland, O., Skeie, R. B., Stier, P., Takemura, T., Tsigaridis, K., Wang, P., Wang, Z., Xu, L., Yu, H., Yu, F., Yoon, J. H., Zhang,

763 K., Zhang, H., and Zhou, C.: Radiative forcing of the direct aerosol effect from AeroCom Phase
764 II simulations, Atmospheric Chemistry and Physics, 13, 1853-1877, 10.5194/acp-13-1853-
765 2013, 2013a.

766 Myhre, G., Shindell, D., Bréon, F.-M., Collins, W., Fuglestvedt, J., Huang, J., Koch, D.,
767 Lamarque, J.-F., Lee, D., Mendoza, B., Nakajima, T., Robock, A., Stephens, G., Takemura, T.,
768 and Zhang, H.: Anthropogenic and Natural Radiative Forcing, in: Climate Change 2013: The
769 Physical Science Basis. Contribution of Working Group I to the Fifth Assessment Report of
770 the Intergovernmental Panel on Climate Change, edited by: Stocker, T. F., Qin, D., Plattner,
771 G.-K., Tignor, M., Allen, S. K., Boschung, J., Nauels, A., Xia, Y., Bex, V., and Midgley, P.
772 M., Cambridge University Press, Cambridge, United Kingdom and New York, NY, USA, 659–
773 740, 2013b.

774 Nasrollahi, N., AghaKouchak, A., Li, J. L., Gao, X. G., Hsu, K. L., and Sorooshian, S.:
775 Assessing the Impacts of Different WRF Precipitation Physics in Hurricane Simulations,
776 Weather and Forecasting, 27, 1003-1016, 10.1175/waf-d-10-05000.1, 2012.

777 Qian, Y., Gustafson Jr, W. I., and Fast, J. D.: An investigation of the sub-grid variability of
778 trace gases and aerosols for global climate modeling, Atmospheric Chemistry and Physics, 10,
779 6917-6946, 10.5194/acp-10-6917-2010, 2010.

780 Rissman, J., Arunachalam, S., Woody, M., West, J. J., BenDor, T., and Binkowski, F. S.: A
781 plume-in-grid approach to characterize air quality impacts of aircraft emissions at the
782 Hartsfield–Jackson Atlanta International Airport, Atmospheric Chemistry and Physics, 13,
783 9285-9302, 10.5194/acp-13-9285-2013, 2013.

784 Rockel, B., Castro, C. L., Pielke, R. A., von Storch, H., and Leoncini, G.: Dynamical
785 downscaling: Assessment of model system dependent retained and added variability for two
786 different regional climate models, Journal of Geophysical Research: Atmospheres, 113,
787 D21107, 10.1029/2007JD009461, 2008.

788 Santarpia, J. L., Gasparini, R., Li, R. J., and Collins, D. R.: Diurnal variations in the
789 hygroscopic growth cycles of ambient aerosol populations, J. Geophys. Res.-Atmos., 110,
790 10.1029/2004jd005279, 2005.

791 Schell, B., Ackermann, I. J., Hass, H., Binkowski, F. S., and Ebel, A.: Modeling the formation
792 of secondary organic aerosol within a comprehensive air quality model system, J. Geophys.
793 Res.-Atmos., 106, 28275-28293, 10.1029/2001jd000384, 2001.

794 Schuster, G. L., Dubovik, O., and Holben, B. N.: Angstrom exponent and bimodal aerosol size
795 distributions, J. Geophys. Res.-Atmos., 111, D07207, doi:10.1029/2005JD006328., 2006.

796 Seinfeld, J. H., and Pandis, S. N.: Atmospheric chemistry and physics: from air pollution to
797 climate change, John Wiley & Sons, 1152 pp., 2016.

798 Simes, R. J.: An improved Bonferroni procedure for multiple tests of significance, Biometrika,
799 73, 751-754, 10.2307/2336545, 1986.

800 Simpson, D., Guenther, A., Hewitt, C. N., and Steinbrecher, R.: Biogenic emissions in Europe.
801 1. estimates and uncertainties, J. Geophys. Res.-Atmos., 100, 22875-22890,
802 10.1029/95jd02368, 1995.

Stocker, T. F. a. Q., D. and Plattner, G.-K. and Alexander, L.V. and Allen, S.K. and Bindoff, N.L. and Bréon, F.-M. and Church, J.A. and Cubasch, U. and Emori, S. and Forster, P. and Friedlingstein, P. and Gillett, N. and Gregory, J.M. and Hartmann, D.L. and Jansen, E. and Kirtman, B. and Knutti, R. and Krishna Kumar, K. and Lemke, P. and Marotzke, J. and Masson-Delmotte, V. and Meehl, G.A. and Mokhov, I.I. and Piao, S. and Ramaswamy, V. and Randall, D. and Rhein, M. and Rojas, M. and Sabine, C. and Shindell, D. and Talley, L.D. and Vaughan, D.G. and Xie, S.-P.: Summary for Policymakers, in: Climate Change 2013: The Physical Science Basis. Contribution of Working Group I to the Fifth Assessment Report of the Intergovernmental Panel on Climate Change, Cambridge University Press, Cambridge, United Kingdom and New York, NY, USA, 33–115, 2013.

Stockwell, W. R., Middleton, P., Chang, J. S., and Tang, X.: The second generation regional acid deposition model chemical mechanism for regional air quality modeling, Journal of Geophysical Research: Atmospheres, 95, 16343-16367, 10.1029/JD095iD10p16343, 1990.

Sun, Y., Yi, L., Zhong, Z., and Ha, Y.: Performance of a New Convective Parameterization Scheme on Model Convergence in Simulations of a Tropical Cyclone at Grey-Zone Resolutions, Journal of the Atmospheric Sciences, 71, 2078-2088, doi:10.1175/JAS-D-13-0285.1, 2014.

Taylor, K. E.: Summarizing multiple aspects of model performance in a single diagram, J. Geophys. Res.-Atmos., 106, 7183-7192, 10.1029/2000jd900719, 2001.

Textor, C., Schulz, M., Guibert, S., Kinne, S., Balkanski, Y., Bauer, S., Berntsen, T., Berglen, T., Boucher, O., Chin, M., Dentener, F., Diehl, T., Easter, R., Feichter, H., Fillmore, D., Ghan, S., Ginoux, P., Gong, S., Kristjansson, J. E., Krol, M., Lauer, A., Lamarque, J. F., Liu, X., Montanaro, V., Myhre, G., Penner, J., Pitari, G., Reddy, S., Seland, O., Stier, P., Takemura, T., and Tie, X.: Analysis and quantification of the diversities of aerosol life cycles within AeroCom, Atmospheric Chemistry and Physics, 6, 1777-1813, 2006.

Tilmes, S., Lamarque, J.-F., Emmons, L., Kinnison, D., Ma, P.-L., Liu, X., Ghan, S., Bardeen, C., Arnold, S., and Deeter, M.: Description and evaluation of tropospheric chemistry and aerosols in the Community Earth System Model (CESM1. 2), Geoscientific Model Development, 8, 1395-1426, doi:10.5194/gmd-8-1395-2015, 2015.

Tomasi, C., Caroli, E., and Vitale, V.: Study of the Relationship between Ångström's Wavelength Exponent and Junge Particle Size Distribution Exponent, Journal of Climate and Applied Meteorology, 22, 1707-1716, 10.1175/1520-0450(1983)022<1707:SOTRBW>2.0.CO;2, 1983.

US-EPA: 2005 National Emissions Inventory (NEI), US Environmental Protection Agency in, available at: ftp://aftp.fsl.noaa.gov/divisions/taq/emissions_data_2005/, 2009.

Vinken, G. C. M., Boersma, K. F., van Donkelaar, A., and Zhang, L.: Constraints on ship NO_x emissions in Europe using GEOS-Chem and OMI satellite NO_2 observations, Atmospheric Chemistry and Physics, 14, 1353-1369, 10.5194/acp-14-1353-2014, 2014.

von Engeln, A., and Teixeira, J.: A Planetary Boundary Layer Height Climatology Derived from ECMWF Reanalysis Data, Journal of Climate, 26, 6575–6590, doi: 10.1175/JCLI-D-12-00385.1, 2013.

Weigum, N., Schutgens, N., and Stier, P.: Effect of aerosol subgrid variability on aerosol optical depth and cloud condensation nuclei: implications for global aerosol modelling, Atmospheric Chemistry and Physics, 16, 13619-13639, 10.5194/acp-16-13619-2016, 2016.

Whitburn, S., Van Damme, M., Clarisse, L., Bauduin, S., Heald, C., Hadji-Lazaro, J., Hurtmans, D., Zondlo, M. A., Clerbaux, C., and Coheur, P.-F.: A flexible and robust neural network IASI-NH_3 retrieval algorithm, J. Geophys. Res.-Atmos., In Press, 10.1002/2016JD024828, 2016.

Wild, O., Zhu, X., and Prather, M. J.: Fast-J: Accurate Simulation of In- and Below-Cloud Photolysis in Tropospheric Chemical Models, Journal of Atmospheric Chemistry, 37, 245-282, 10.1023/a:1006415919030, 2000.

Zhang, X., Chen, Z. M., Wang, H. L., He, S. Z., and Huang, D. M.: An important pathway for ozonolysis of alpha-pinene and beta-pinene in aqueous phase and its atmospheric implications, Atmospheric Environment, 43, 4465-4471, 10.1016/j.atmosenv.2009.06.028, 2009.

Zhang, Y., He, J., Zhu, S., and Gantt, B.: Sensitivity of simulated chemical concentrations and aerosol-meteorology interactions to aerosol treatments and biogenic organic emissions in WRF/Chem, Journal of Geophysical Research: Atmospheres, 121, 6014-6048, 10.1002/2016JD024882, 2016.

Zieger, P., Fierz-Schmidhauser, R., Weingartner, E., and Baltensperger, U.: Effects of relative humidity on aerosol light scattering: results from different European sites, Atmospheric Chemistry and Physics, 13, 10609-10631, 10.5194/acp-13-10609-2013, 2013.

Figures

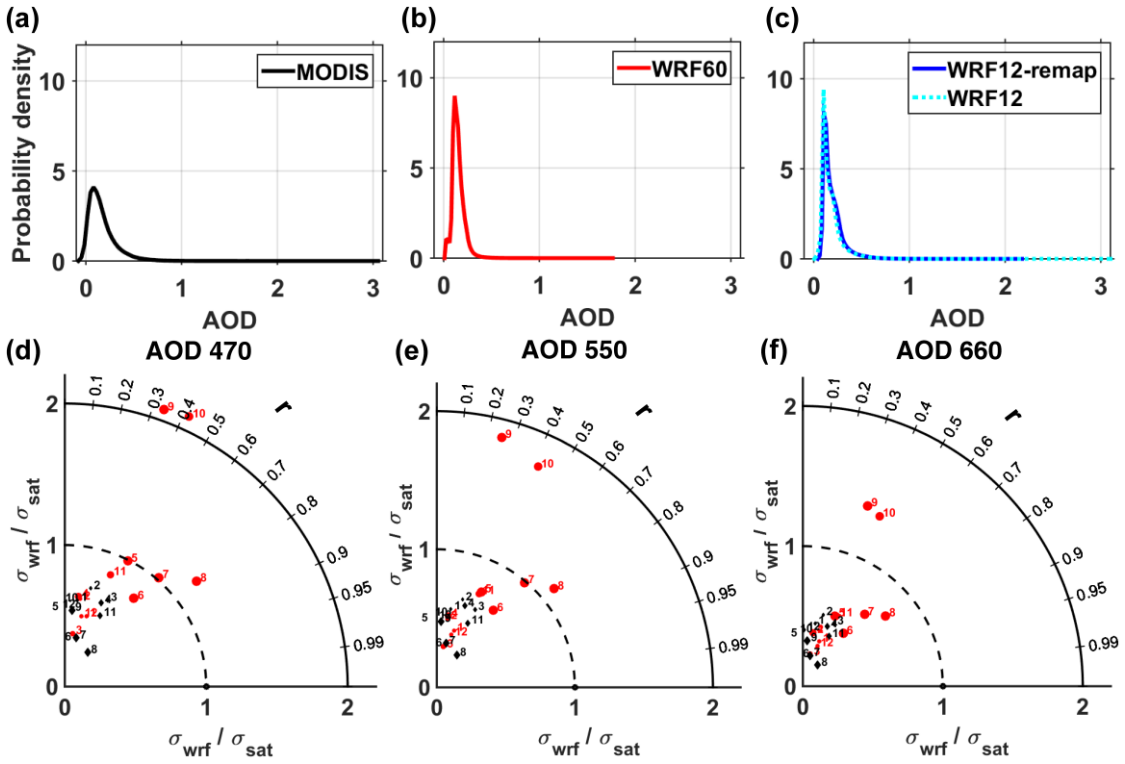

Figure 1. Probability density function of once daily AOD at a wavelength (λ) of 550 nm for (a) MODIS, (b) WRF60 and (c) WRF12 and WRF12-remap during the year 2008. (d-f) Taylor diagrams of mean monthly AOD at wavelengths (λ) of (d) 470, (e) 550 and (f) 660 nm as simulated by WRF-Chem at different resolutions (black diamonds=WRF60 and red dots=WRF12-remap) relative to MODIS observations. The numbers by each symbol denote the calendar month (e.g. 1=January).

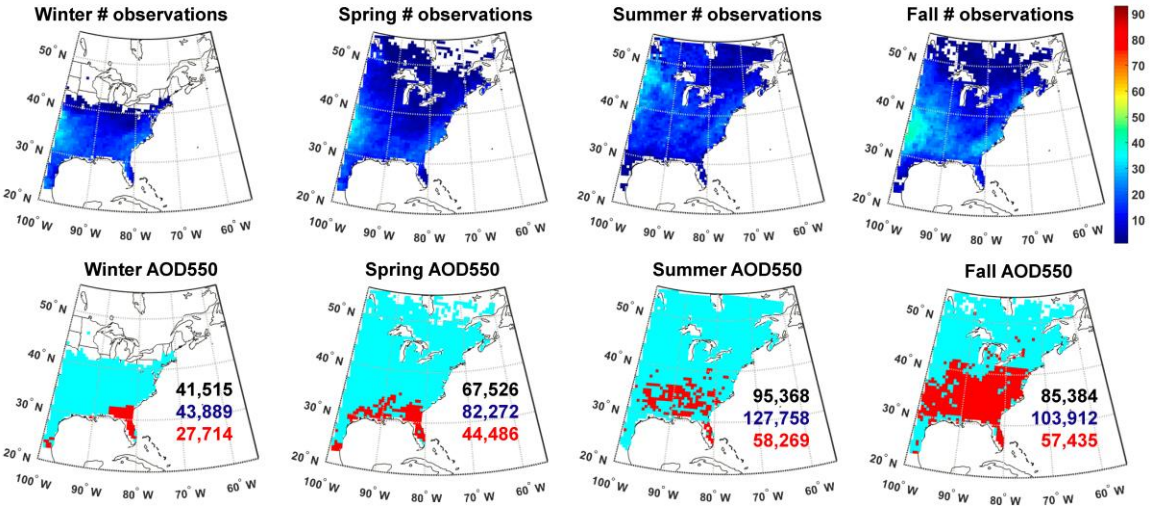

Figure 2. First line: Number of paired AOD observations at a wavelength (λ) of 550 nm (i.e. simultaneous values as output from WRF-Chem and observed by MODIS) used to perform a t-test designed to evaluate whether the difference computed for each grid cell as WRF60-MODIS differs from that computed as WRF12-remap-MODIS on a seasonal basis (columns show Winter (DJF), Spring (MAM), Summer (JJA) and Fall (SON)). Second line: Results of the t-test. Pixels that have p-values that are significantly different at α=0.10 are indicated in red and have been corrected for multiple testing using a False Discovery Rate approach. The number of observations of cloud-free conditions summed across all days in each season and all grid cells is also reported (black=MODIS, blue=WRF60, red=WRF12-remap).

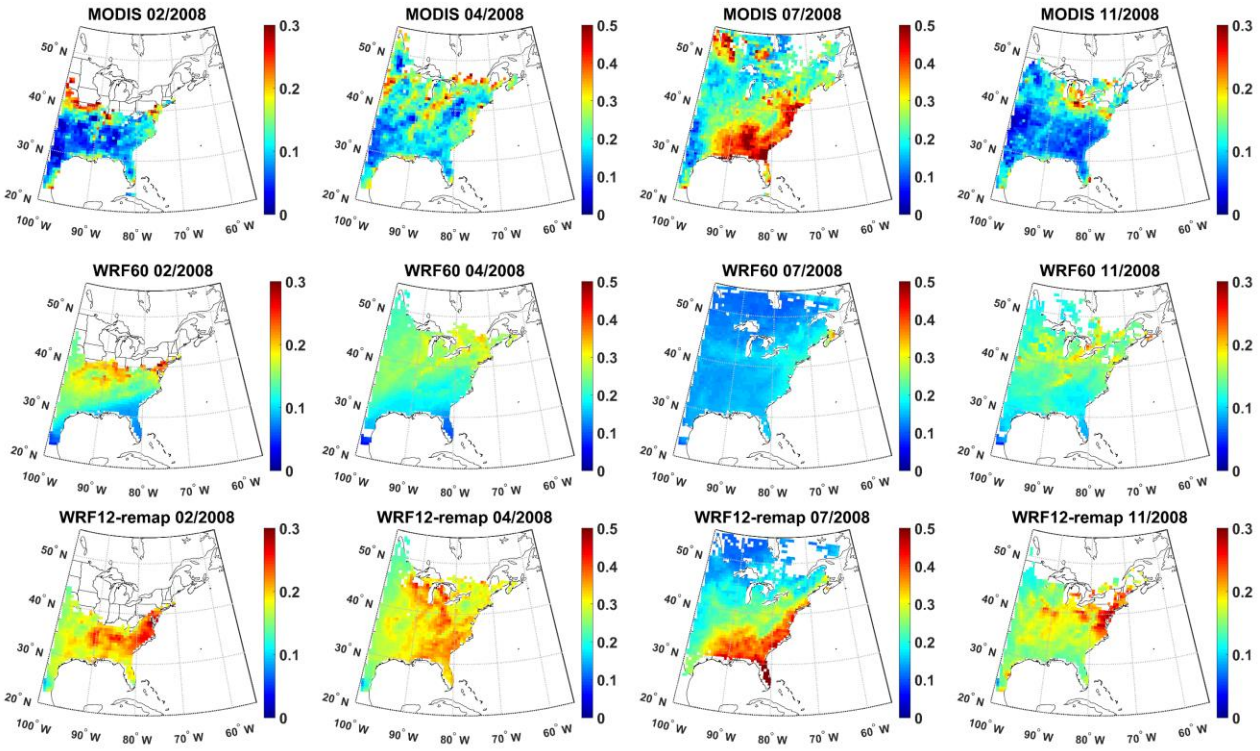

888

889 **Figure 3. Monthly mean AOD at a wavelength (λ) of 550 nm from MODIS (first line) and**
890 **WRF-Chem at different resolutions (WRF60 and WRF12-remap, second and third line)**
891 **during a representative month in each climatological season (columns). Note that a**
892 **different color scale is applied for different months. For a monthly mean value for a grid**
893 **cell to be shown, there must be at least 5-simultaneous daily values (for the time of the**
894 **satellite overpass) available.**

895

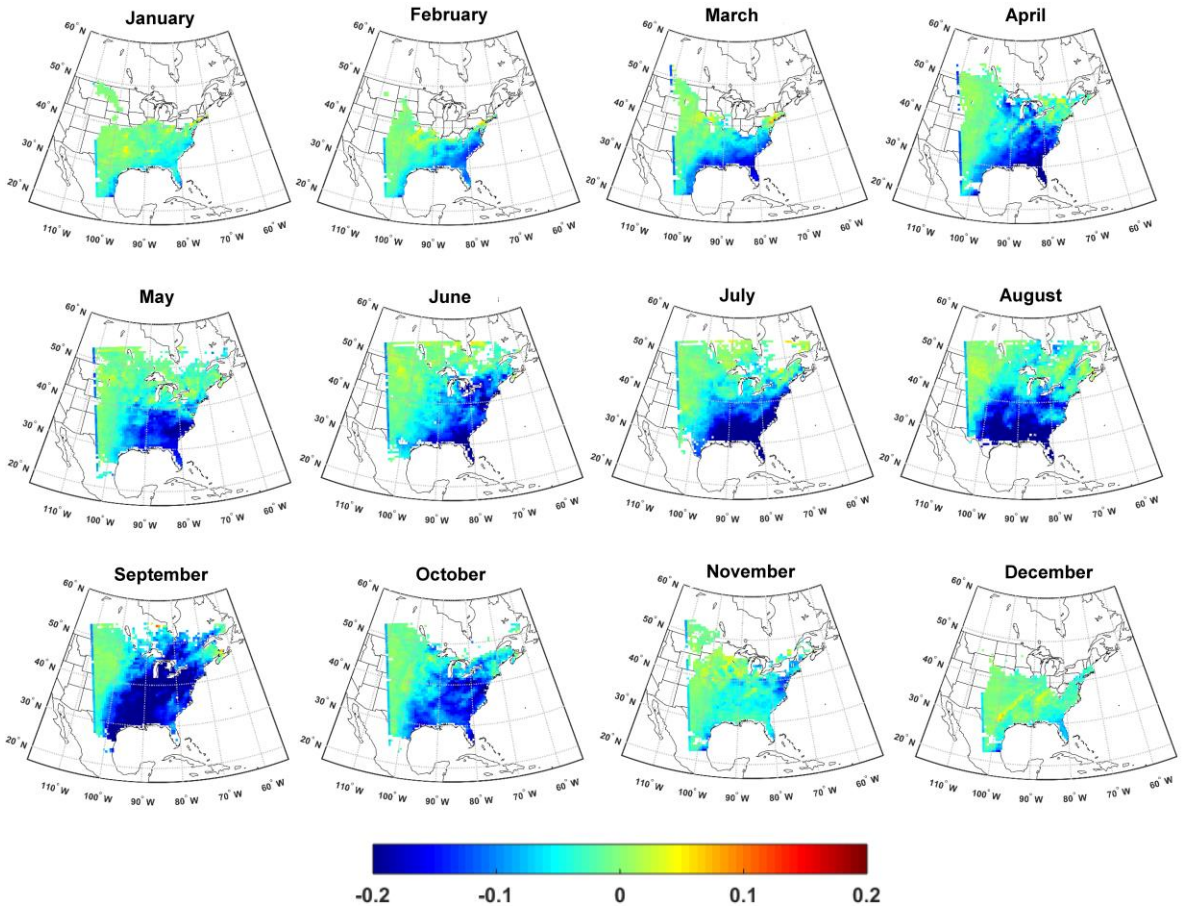

Figure 4. Difference in monthly mean AOD at a wavelength (λ) of 550 nm between WRF-Chem simulations conducted at 60 km resolution (WRF60) and output from WRF-Chem simulations conducted with a resolution of 12 km but remapped to 60 km (WRF12-remap). Differences are computed as WRF60 minus WRF12-remap. Similar spatial patterns and magnitudes of differences are found for λ of 470 and 660 nm. The calendar months of 2008 are shown in the titles of each panel.

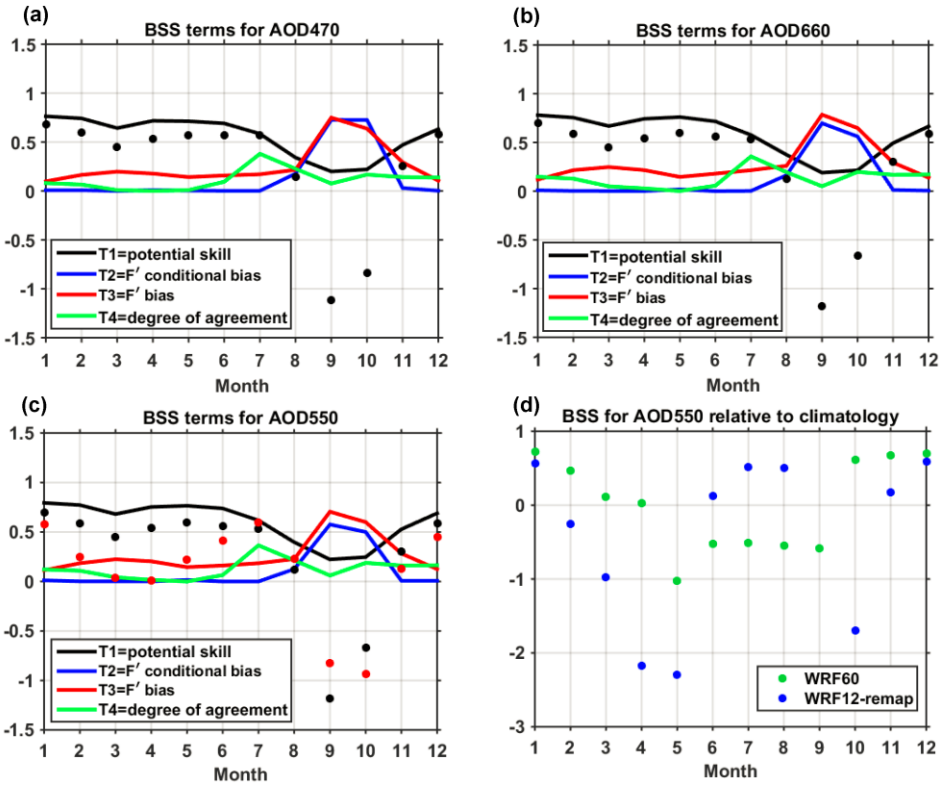

Figure 5. (a-c) Brier Skill Scores (BSS, black dots) for monthly mean AOD by calendar month (1=January) for AOD at 470, 550 and 660 nm. In this analysis of model skill WRF12 output is mapped to the WRF60 grid (WRF12-remap) and BSS are computed using MODIS as the target, WRF60 (driven by NAM12 meteorological boundary conditions) as the reference forecast and WRF12-remap as the forecast. Also shown by the color lines are the contributions of different terms to BSS. In panel c the red dots indicate BSS when the reference forecast is WRF60 driven by GFS meteorological boundary conditions. (d) BSS of monthly mean AOD from WRF60 (green dots) and WRF12-remap (blue dots) relative to MODIS monthly mean climatology during 2000-2014 (reference forecast). Monthly mean AOD from MODIS are used as the target. BSS for WRF12-remap in September is -6.1.

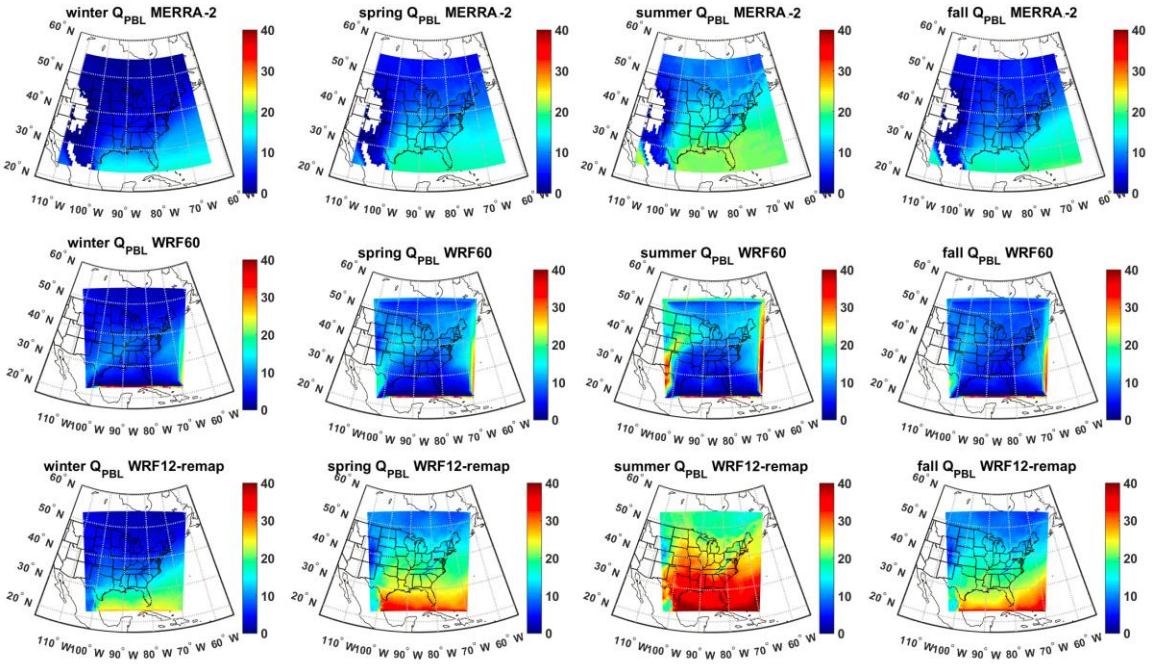

Figure 6. Seasonal mean specific humidity [kg m^{-2}] integrated from the surface to 825 hPa (Q_{PBL}) from MERRA-2 (first row) assuming an average air density in the *PBL* of 1.1 kg m^{-3}, WRF60 (second row), and WRF12-remap (third row). The data are 3-hourly and show only cloud-free hours in all three data sets.

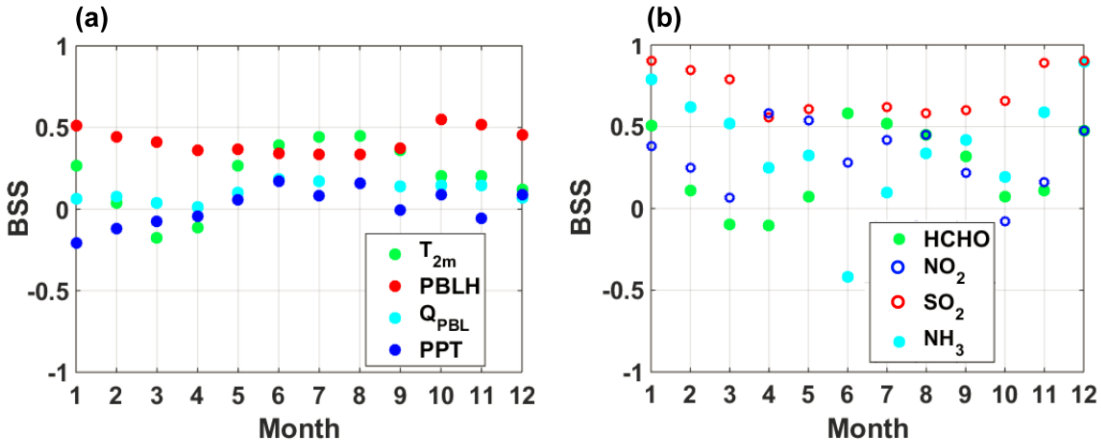

924

925 **Figure 7. Brier Skill Scores (BSS) for key (a) meteorological and (b) chemical variables.**
926 **BSS are computed using hourly data of T at 2m (T_{2m}) and *PBLH*, 3-hourly estimates of**
927 **specific humidity in the boundary layer (Q_{PBL}), and z-scores of monthly total precipitation**
928 **(*PPT*), and of monthly mean columnar gas phase concentrations.**

929

930

Tables

Table 1. Physical and chemical schemes adopted in the WRF-Chem simulations presented herein.

Simulation settings	**Values**
Domain size	300 × 300 (60 × 60) grid points
Horizontal resolution	12 km (60 km)
Vertical resolution	32 levels up to 50 hPa
Timestep for physics	72 s (300 s)
Timestep for chemistry	5 s
Physics option	**Adopted scheme**
Microphysics	WRF Single-Moment 5-class (Hong et al., 2004)
Longwave Radiation	Rapid Radiative Transfer Model (RRTM) (Mlawer et al., 1997)
Shortwave Radiation	Goddard (Fast et al., 2006)
Surface layer	Monin Obhukov similarity (Janjić, 2002;Janjić, 1994)
Land Surface	Noah Land Surface Model (Chen and Dudhia, 2001)
Planetary boundary layer	Mellor-Yamada-Janjich (Janjić, 1994)
Cumulus parameterizations	Grell 3D (Grell and Dévényi, 2002)
Chemistry option	**Adopted scheme**
Photolysis	Fast J (Wild et al., 2000)
Gas-phase chemistry	RADM2 (Stockwell et al., 1990)
Aerosols	MADE/SORGAM (Ackermann et al., 1998;Schell et al., 2001)
Anthropogenic emissions	NEI (2005) (US-EPA, 2009)
Biogenic emissions	Guenther, from USGS land use classification (Guenther et al., 1994;Guenther et al., 1993;Simpson et al., 1995)

Table 2. Spearman correlation coefficients (ρ) between AOD at wavelengths (λ) of 470, 550 and 660 nm from MODIS observations averaged over 12 or 60 km and WRF-Chem simulations conducted at 60 km (WRF60, shown in the table as -60), at 12 km (WRF12, shown in the table as -12), and from WRF-Chem simulations at 12 km but remapped to 60 km (WRF12-remap, shown in the table as -remap). Given WRF12-remap is obtained by averaging WRF12 when at least half of the 5×5 12 km resolution cells contain valid data, ρ from WRF60 and WRF12-remap may be computed on slightly different observations and sample size. The bold text denotes correlation coefficients that are significant at α=0.05 after a Bonferroni correction is applied (i.e. $p \le \frac{0.05}{9 \times 12} = 4.63 \times 10^{-4}$ **is significant). The yellow shading is a visual guide that shows for each month and λ the model output that has highest ρ with MODIS.**

Month→/ Variable↓	Jan	Feb	Mar	Apr	May	Jun	Jul	Aug	Sep	Oct	Nov	Dec
470-12	**0.238**	**0.150**	**0.137**	**0.147**	**0.377**	**0.581**	**0.610**	**0.723**	**0.352**	**0.306**	**0.259**	**0.212**
470-60	0.156	**0.226**	**0.438**	**0.412**	**-0.219**	**-0.146**	**0.379**	**0.601**	0.087	-0.051	**0.500**	-0.059
470-remap	**0.295**	**0.197**	**0.250**	**0.182**	**0.516**	**0.637**	**0.675**	**0.777**	**0.368**	**0.441**	**0.315**	**0.274**
550-12	**0.223**	**0.124**	**0.142**	**0.146**	**0.349**	**0.541**	**0.580**	**0.689**	**0.275**	**0.301**	**0.280**	**0.215**
550-60	**0.179**	**0.244**	**0.429**	**0.332**	**-0.288**	**-0.188**	**0.324**	0.567	0.073	-0.077	**0.491**	0.002
550-remap	**0.297**	0.164	**0.261**	**0.199**	**0.493**	**0.605**	**0.651**	**0.747**	**0.286**	**0.437**	**0.352**	**0.309**
660-12	**0.217**	**0.136**	**0.165**	**0.152**	**0.324**	**0.476**	**0.540**	**0.644**	**0.183**	**0.290**	**0.292**	**0.221**
660-60	**0.191**	**0.230**	**0.437**	**0.402**	**-0.305**	**-0.189**	**0.389**	**0.616**	0.099	**-0.137**	**0.536**	0.049
660-remap	**0.356**	**0.211**	**0.289**	**0.208**	**0.480**	**0.624**	**0.669**	**0.772**	**0.371**	**0.432**	**0.393**	**0.368**

Table 3. Spatial coherence in the identification of extreme AOD values (i.e. areas with AOD>75th percentile over space for each month) between WRF-Chem at different resolutions relative to MODIS. No significant wavelength dependence is found for model skill in identifying extreme AOD so results are only shown for λ = 550 nm. The different model output is denoted by -60 for simulations at 60 km, -12 for simulations at 12 km resolution, and as –remap for simulations at 12 km but with the output remapped to 60 km. The *Accuracy* (Acc) indicates the fraction of grid cells co-identified as extremes and non-extremes between WRF-Chem and MODIS relative to the total number of cells with valid data. The *Hit Rate* (*HR*) is the probability of correct forecast and is the proportion of cells correctly identified as extremes by both WRF-Chem and MODIS. The yellow shading indicates the model resolution with highest skill in each month for AOD at 550 nm.

Month→/ Metric↓	Jan	Feb	Mar	Apr	May	Jun	Jul	Aug	Sep	Oct	Nov	Dec
Acc-12	0.673	0.665	0.659	0.638	0.710	0.800	0.855	0.839	0.666	0.679	0.723	0.661
Acc-60	0.707	0.778	0.735	0.730	0.600	0.587	0.658	0.769	0.661	0.637	0.729	0.681
Acc-remap	0.674	0.680	0.694	0.640	0.766	0.824	0.887	0.837	0.667	0.699	0.767	0.641
HR-12	0.346	0.331	0.319	0.275	0.421	0.599	0.711	0.678	0.333	0.358	0.447	0.323
HR-60	0.417	0.558	0.471	0.460	0.200	0.173	0.315	0.538	0.321	0.274	0.458	0.364
HR-remap	0.350	0.361	0.387	0.281	0.532	0.649	0.775	0.674	0.333	0.399	0.535	0.284